Acta Materialia 230 (2022) 117778

Contents lists available at ScienceDirect

Acta Materialia

journal homepage: www.elsevier.com/locate/actamat

Full length article

Ab initio-guided X-ray photoelectron spectroscopy quantification of Ti vacancies in $Ti_{1-\delta}O_xN_{1-x}$ thin films

Pavel Ondračka[a,*], Marcus Hans[a], Damian M. Holzapfel[a], Daniel Primetzhofer[b], David Holec[c], Jochen M. Schneider[a]

[a] Materials Chemistry, RWTH Aachen University, Kopernikusstr. 10, D-52074 Aachen, Germany
[b] Department of Physics and Astronomy, Uppsala University, Lägerhyddsvägen 1, S-75120 Uppsala, Sweden
[c] Department of Materials Science, Montanuniversität Leoben, Franz-Josef-Strasse 18, A-8700 Leoben, Austria

ARTICLE INFO

Article history:
Received 27 October 2021
Revised 11 February 2022
Accepted 18 February 2022
Available online 24 February 2022

Keywords:
$Ti_{1-\delta}O_xN_{1-x}$
Ti vacancy
Vacancy concentration quantification
X-ray photoelectron spectroscopy
Density functional theory

ABSTRACT

Ab initio calculations were employed to investigate the effect of oxygen concentration dependent Ti vacancies formation on the core electron binding energy shifts in cubic titanium oxynitride ($Ti_{1-\delta}O_xN_{1-x}$). It was shown, that the presence of a Ti vacancy reduces the 1s core electron binding energy of the first N neighbors by ~ 0.6 eV and that this effect is additive with respect to the number of vacancies. Hence it is predicted that the Ti vacancy concentration can be revealed from the intensity of the shifted components in the N 1s core spectra region. This notion was critically appraised by fitting the N 1s region obtained via X-ray photoelectron spectroscopy (XPS) measurements of $Ti_{1-\delta}O_xN_{1-x}$ thin films deposited by high power pulsed magnetron sputtering. A model to quantify the Ti vacancy concentration based on the intensity ratio between the N 1s signal components, corresponding to N atoms with locally different Ti vacancy concentration, was developed. Herein a random vacancy distribution was assumed and the influence of surface oxidation from atmospheric exposure after deposition was considered. The so estimated vacancy concentrations are consistent with a model calculating the vacancy concentration based on the O concentrations determined by elastic recoil detection analysis and text book oxidation states and hence electroneutrality. Thus, we have unequivocally established that the formation and population of Ti vacancies in cubic $Ti_{1-\delta}O_xN_{1-x}$ thin films can be quantified by XPS measurements from N 1s core electron binding energy shifts.

1. Introduction

It is generally accepted that point defects affect stability and mechanical properties of nitrides and oxynitrides [1–3]. Nitrogen vacancies were used previously to increase hardness in TiN_x films [4,5] and toughness in $V_{0.5}Mo_{0.5}N_x$ [6]. Another example of point defect engineering are efforts to improve temperature stability in TiAlN [7]. Furthermore, it was shown that nitrogen vacancies can be used to stabilize the mechanically unstable cubic MoN [8], TaN [8] and WN [9]. Theoretically, point defects are readily described, however, precise point defect quantification is a challenging experimental task and is usually done via indirect estimates such as composition and/or lattice parameter measurements [1,7]. While positron annihilation spectroscopy can quantify defects like vacancies or dislocations, a knowledge of lifetime for positrons annihilated in the bulk (defect free) material is required [10].

However, since it was established that the coordination number of an atom influences the core electron binding energies (BE) [11], it is possible to detect and quantify the point defect concentration by using X-ray photoelectron spectroscopy (XPS), provided that the population of point defects and the corresponding energy shift can be resolved spectroscopically. One material class with inherently high point defect concentrations are rocksalt structure oxynitrides. It was shown that the presence of oxygen induces metal vacancies in significant concentrations in VAlON [12] and TiAlON [1,13,14] and more specifically, that the vacancy concentration depends directly on the oxygen content based on a simple textbook oxidation state electroneutrality model (1 Ti vacancy per 3 O atoms) [1,12]. Therefore, the oxynitrides are selected for a critical appraisal of the XPS-based vacancy detection and quantification notion.

In recent years, the importance of *ab initio* calculations in analysis and understanding of the X-ray photoelectron spectroscopy measurements has been growing. Some recent examples include studies of poly-epoxy polymer surface bonding [15–17] determi-

* Corresponding author.
E-mail address: pavel.ondracka@gmail.com (P. Ondračka).

https://doi.org/10.1016/j.actamat.2022.117778

nation of N-doping positions in TiO_2 [18], determination of the structure of epitaxially grown silicene [19], efforts to distinguish the amount of O in TiO_2, mixed TiSi and SiO_2-like environment, allowing quantification of Ti and Si mixing in the $Ti_xSi_{1-x}O_2$ thin films [20] and others [21–23].

In this work, we combine *ab initio* density functional theory (DFT) calculations and XPS measurements to critically appraise if the presence and population of Ti vacancies can be resolved by XPS in $Ti_{1-\delta}O_xN_{1-x}$ thin films with varying O content.

2. Methodology

$Ti_{1-\delta}O_xN_{1-x}$ thin films were deposited using reactive high power pulsed magnetron sputtering (HPPMS) utilizing a combinatorial setup [24]. Si (100) substrates were positioned at a distance of 10 cm with respect to the cathode. Oxygen was introduced at the top of the 0.5 m long cathode to achieve a gradient in the partial oxygen pressure over the cathode length. Consequently, a chemical composition spread was realized on the substrates as a function of the distance from the oxygen inlet. The base pressure was always $< 9 \times 10^{-5}$ Pa and increased to $< 2.5 \times 10^{-4}$ Pa after heating the substrates to ~ 380 °C. The Ar (purity > 99.999%) flow was set to 200 square cubic centimeter per minute (sccm) and N_2 (purity > 99.999%) flow was 30 sccm, leading to total pressure of approximately 0.43 Pa for all depositions. The Ti target (purity > 99 wt.%) was sputtered at a duty cycle of 2.5% and at a frequency of 500 Hz (20 µs on time, 1950 µs off time), with a time-average power of 1485 W. The depositions were done in four batches, using 0, 0.45, 0.9 and 1.35 sccm of O_2 flow (purity > 99.999%) respectively, leading to peak currents of 229, 229, 219 and 208 A and peak power densities of 361, 367, 348 and 333 Wcm^{-2} for the respective batches. The Si substrates were kept at a floating potential. After 90 min depositions, the samples were cooled in vacuum for at least 4 h and only vented when the sample holder temperature was below 60 °C in order to minimize the surface oxidation after deposition [25].

XPS measurements were carried out in a KRATOS AXIS SUPRA spectrometer, using an Al K_α monochromatic source at 1486.6 eV, hemispherical analyzer and 128-channel delay-line detector. High resolution spectra of the N 1s region were taken using the pass energy of 10 eV, energy step of 0.04 eV, integration time of 1 s and 12 sweeps. The measurements were done in hybrid mode with the measurement spot size of 700 × 300 µm. All of the samples were sufficiently conductive and no charging was observed. The BE scale of the spectrometer was calibrated using the sputter-cleaned polycrystalline Ag foil, leading to Ag $3d_{5/2}$ peak position at 368.2 eV. Chemical composition depth profiling was done by time-of-flight elastic recoil detection analysis (ERDA) at the Tandem Laboratory of Uppsala University and details can be found in Azina et al. [26]. Nitrogen concentrations were corrected based on a stoichiometric TiN reference thin film [27]. Average chemical compositions were obtained from the depth profiles by excluding the surface-near region. The statistical uncertainty in all measured depth profiles was < 0.4 at.%. In this manuscript all samples are referred to by their O concentration as measured by ERDA. X-ray diffraction (XRD) measurements were done with a Bruker D8 Discovery general area detector diffraction system (GADDS) using Cu($K\alpha$) radiation. More detailed information pertaining to experimental procedures employed can be found in the Supplementary material (SM).

Density functional theory [28,29] was employed for the calculations of BE shifts. $Ti_{1-\delta}O_xN_{1-x}$ 2 × 2 × 2 supercells based on the NaCl-type TiN conventional cubic cell were generated using the special quasi-random structure (SQS) method [30] for the electroneutral configurations, specifically with 1 Ti vacancy per 3 O atoms. Six different compositions with 0, 3, 6, 9, 12 and 15 O atoms per cell were considered. Additionally, configurations with 1, 2 and 4 extra Ti vacancies (no longer maintaining the electroneutrality) were generated containing the same number of oxygen atoms as the electroneutral configurations. Three SQS structures were constructed for every composition and the quantities reported here are the average from the three different cells. Vienna *ab initio* package was used for the full structural relaxation of all cells [31,32]. A core-hole approach was used for the calculation of the binding energies of the core level [11]. The binding energy was calculated as an energy difference between final state, where electron from the specific core level was placed into the valence band, and the initial ground state. This method, although not yielding accurate absolute BE values, is able to provide precise BE differences. BEs were calculated for N 1s states of all atoms in the electroneutral structures using the Wien2k full-potential all electron code [33]. Specific implementation and numerical details of the calculations are described in the SM Section S1 and all calculated data are available under the Creative Commons license in the NOMAD archive [34].

3. Results and discussion

All as deposited $Ti_{1-\delta}O_xN_{1-x}$ films with varying O concentrations ranging from 0.4 at.% to 28.6 at.% (SM Table S6), as determined by ERDA measurements, exhibit a single cubic phase based on XRD (SM Figure S3). The film morphology changes from dense columnar grains for samples with low O content to a fine-grained nanocrystalline microstructure as more O is incorporated (SM Figure S7). Further details and discussion about the film composition and structure can be found in SM Sections S3, S4 and S5.

N 1s core level XPS measurements of selected samples are presented in Fig. 1. As the O content increases, significant shifts of the spectral weights to lower BEs are clearly visible. Qualitatively, this is consistent with previous reports on TiN surface oxidation, where the surface oxynitride component was reported at lower binding energies with respect to the main TiN component [25,35]. The decreasing intensity of the N 1s signal is caused by the overall decrease of the N content as a consequence of the substitution by O.

For fitting of the N 1s XPS data we modified the approach from Greczynski and Hultman [35]. Here, minor differences include a Tougaard-like background [36] and the separation of single TiO_xN_y component into two components $TiON^1$ and $TiON^2$ was implemented, as reasonable fits using four peaks only from [35] in the case of TiN-oxidation, namely TiN, TiN-sat, TiO_xN_y and N_2 could not be obtained. However, a fitting procedure using an additional TiON peak (TiN, $TiON^1$, $TiON^2$, TiN-sat and N_2), resulted in high quality fits for all studied compositions. An example fit for one selected composition is presented in Fig. 2(a) and shows that all

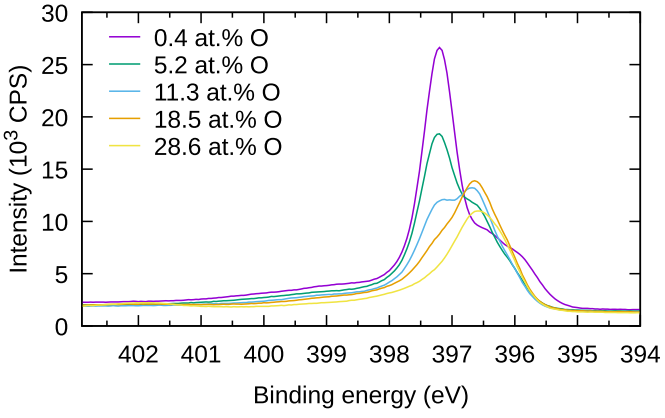

Fig. 1. Selected measured N 1s XPS spectra.

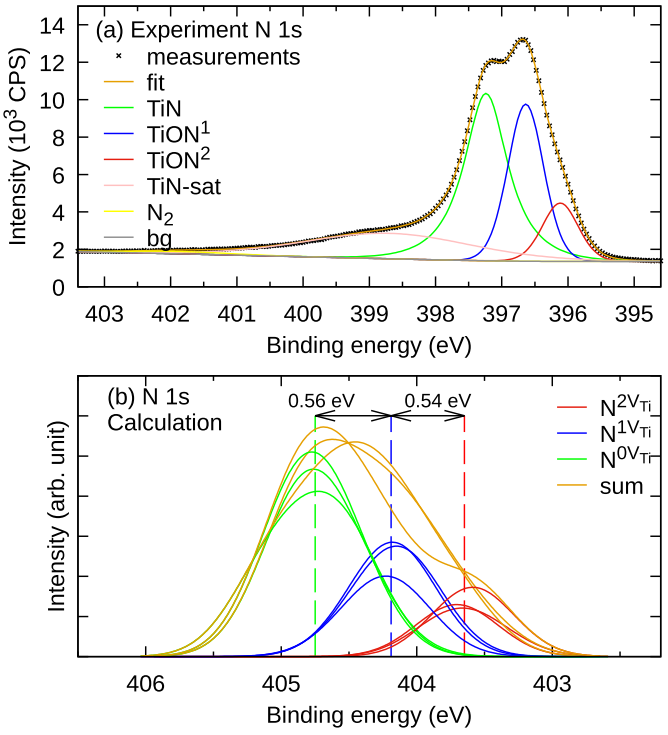

Fig. 2. (a) Example fit of the N 1s spectra for the sample with 11.3 at.% O. Fits of other compositions can be found in SM Figure S9. (b) Calculated N 1s broadened binding energies for electroneutral $Ti_{1-\delta}O_xN_{1-x}$ with 14.7 at.% of O. Three lines correspond to three different SQS cells with the same composition. The lines were produced by replacing the calculated discrete binding energies by Gaussians at the same energy position with $\sigma = 0.3$ eV to produce spectral-like curves for the sole purpose of visual comparison with the experimental spectra. The dashed lines correspond to mean BE values for the specific components. All calculated compositions are shown in SM Figure S2.

of the components are well distinguishable. Gaussian–Lorentzian symmetric peak shapes in a product form with 30% Lorentzian ratio were used for four of the fitted components, with the exception of the TiN component, where consistently with Greczynski and Hultman [35] a 90% Lorentzian ratio was used. Our main motivation for choosing the here employed line shapes was to keep the fit as simple as possible and to allow for a straightforward and consistent comparison with previously published work by Greczynski and Hultman [35]. Also, from the data depicted in Fig. 2(a) and SM Figure S9 it is evident that the here employed line shapes result in very good fits to the experimental data for all compositions. This is further illustrated by the small binding energy and component ratios fitting uncertainties indicated in Fig. 3a and Fig. 4(a) respectively. Intensity, width and position (mean BE) of the five components were free parameters during the fitting, while the width of the $TiON^1$ was fixed to be the same as of the $TiON^2$, to reduce the number of free parameters. It was not possible to fit the position of the N_2 component as it was too weak in some compositions leading to ambiguity, however this was solved by performing a multi-sample fit, i.e., fitting all the compositions at the same time with the position of the N_2 component as a free parameter but shared by all compositions. This resulted in a value of 401.86 eV for N_2, very close to the reported value of 401.80 eV from Greczynski and Hultman [35].

The fitted mean BEs of the TiN, $TiON^1$, and $TiON^2$ components are shown in Fig. 3(a) and Table 1. The BE differences between the TiN and $TiON^1$ BEs are approximately 0.6 eV for most compositions, while the differences between the $TiON^1$ and $TiON^2$ BEs are slightly smaller, approximately 0.5 eV.

Table 1
Fitted XPS N 1s component ratios and mean BEs for all samples as well as the mean BE differences between the TiN, $TiON^1$ and $TiON^2$ components.

[O] (at.%)	f^{TiN} (%)	f^{TiON^1} (%)	f^{TiON^2} (%)	f^{sat} (%)	f_2^N (%)	E^{TiN} (eV)	E^{TiON^1} (eV)	E^{TiON^2} (eV)	E^{sat} (eV)	E^{N_2} (eV)	$E^{TiN} - E^{TiON^1}$ (eV)	$E^{TiON^2} - E^{TiON^1}$ (eV)
0.4	63.0	10.0	8.1	17.6	1.3	397.20	396.37	395.85	398.97	401.86	0.83	0.52
3.1	60.2	12.1	6.7	20.0	1.0	397.21	396.53	396.03	398.92	401.86	0.68	0.50
4.1	57.8	14.3	7.3	19.6	1.0	397.22	396.56	396.05	398.90	401.86	0.67	0.51
5.2	54.9	16.8	7.6	19.7	0.9	397.23	396.59	396.07	398.88	401.86	0.64	0.52
7.4	49.2	21.3	8.4	20.2	0.9	397.24	396.62	396.09	398.82	401.86	0.62	0.53
10.1	45.3	25.2	9.1	19.3	1.1	397.24	396.64	396.11	398.81	401.86	0.61	0.53
11.3	41.2	27.2	10.1	20.4	1.1	397.24	396.64	396.12	398.71	401.86	0.60	0.52
11.6	43.3	26.6	9.8	19.2	1.2	397.23	396.64	396.12	398.77	401.86	0.60	0.52
16.5	34.4	30.0	13.0	20.6	2.0	397.22	396.64	396.14	398.53	401.86	0.57	0.50
16.8	36.9	29.0	13.3	18.5	2.3	397.20	396.64	396.14	398.63	401.86	0.56	0.50
17.6	35.4	29.4	13.9	18.6	2.7	397.19	396.64	396.14	398.56	401.86	0.56	0.50
18.5	32.1	31.0	15.0	19.3	2.6	397.20	396.63	396.14	398.41	401.86	0.56	0.49
20.6	31.7	29.8	16.7	17.6	4.2	397.18	396.64	396.15	398.40	401.86	0.54	0.49
22.3	30.2	30.2	17.9	17.0	4.7	397.18	396.64	396.16	398.37	401.86	0.54	0.48
24.2	28.0	30.9	19.3	17.2	4.7	397.20	396.66	396.18	398.30	401.86	0.55	0.48
26.4	27.6	30.7	21.0	15.4	5.2	397.22	396.66	396.19	398.36	401.86	0.56	0.47
28.6	25.0	31.6	23.2	14.8	5.4	397.26	396.67	396.20	398.33	401.86	0.59	0.47
mean difference:											0.60	0.50

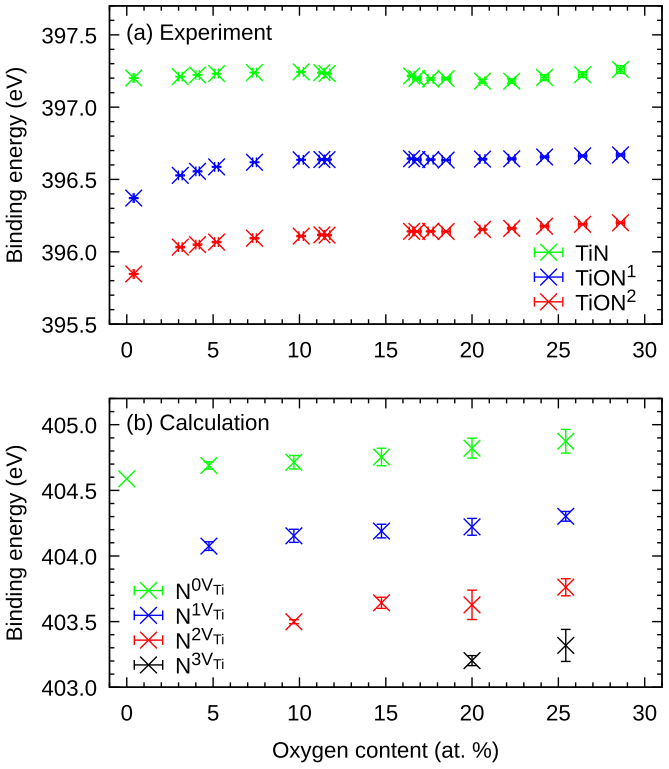

Fig. 3. Evolution of (a) fitted positions of the TiN, $TiON^1$ and $TiON^2$ components, (b) calculated mean binding energies of $N^{0V_{Ti}}$, $N^{1V_{Ti}}$, $N^{2V_{Ti}}$ and $N^{3V_{Ti}}$ components, as a function of O content.

DFT calculations were employed to critically appraise the working hypothesis of this paper, namely that the presence of Ti vacancies causes significant and hence measurable changes in the N 1s core level binding energies and that subsequently the population of defects can be quantified by XPS. For evaluation of the N 1s core levels, the calculated binding energies of all N atoms in the structure were hence divided into groups based on the number of Ti vacancies in the first coordination shell. Nitrogen with 6 Ti neighbors and 0 Ti vacancies is being labeled as $N^{0V_{Ti}}$, while $N^{1V_{Ti}}$ has 5 Ti neighbors and 1 Ti vacancy, etc., see Fig. 5. Fig. 2(b) shows a broadened calculated binding energies of the N 1s core levels for the electroneutral $Ti_{1-\delta}O_xN_{1-x}$ with 14.8 at.% of O. The binding energies for $N^{1V_{Ti}}$ and $N^{2V_{Ti}}$ atoms are shifted to smaller binding energies by 0.56 eV and 1.1 eV with respect to the main $N^{0V_{Ti}}$ component, respectively. The evolution of mean $N^{0V_{Ti}}$, $N^{1V_{Ti}}$, $N^{2V_{Ti}}$ and $N^{3V_{Ti}}$ N 1s binding energies as a function of O content for all calculated compositions is shown in Fig. 3(b). The peak positions of the individual $N^{nV_{Ti}}$ components shift to a slightly higher BEs as the oxygen content increases, however the overall shift is below 0.2 eV over the whole oxygen concentration range. The shifts between the different $N^{nV_{Ti}}$ components corresponding to the different numbers of vacancies are, however, very similar for all compositions. This suggests that the relative BE shifts do not depend on the overall composition of the films, but are sensitive to the specific local chemical environment. Furthermore, it is evident that the effect of the Ti vacancies on the N 1s core level is additive and amounts to 0.5–0.6 eV BE decrease per Ti vacancy in the first coordination shell. Therefore, the calculated binding energies predict a significant shift of the N 1s core level, due to the presence of Ti vacancies in the first coordination shell which is consistent with our working hypothesis that the presence and population of Ti vacancies in $Ti_{1-\delta}O_xN_{1-x}$ thin films can be quantified by the XPS measurements.

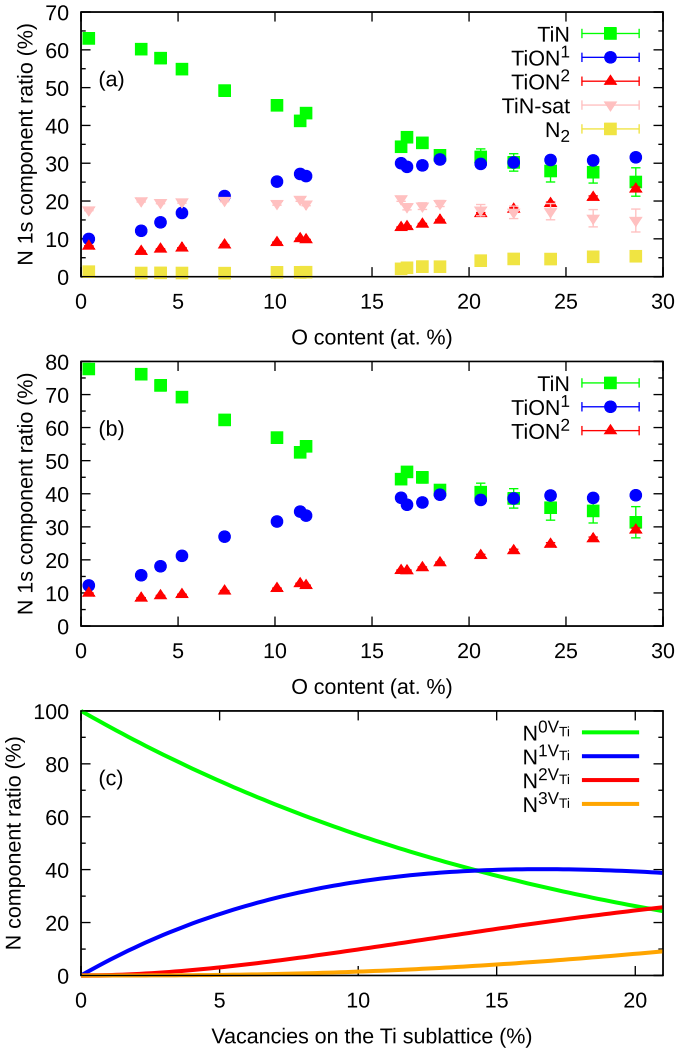

Fig. 4. (a) Oxygen dependent N 1s component evolution, (b) TiN, $TiON^1$, and $TiON^2$ components renormalized to 1, (c) theoretical dependency of the $N^{0V_{Ti}}$, $N^{1V_{Ti}}$, and $N^{2V_{Ti}}$ components, under the assumption of random vacancy distribution.

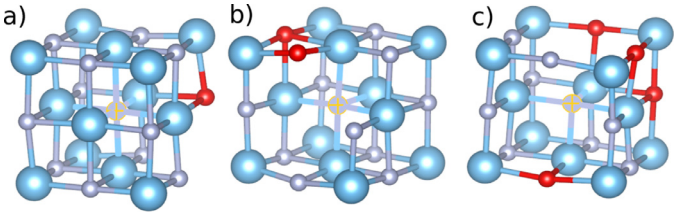

Fig. 5. Example of (a) $N^{0V_{Ti}}$, (b) $N^{1V_{Ti}}$ and (c) $N^{2V_{Ti}}$ atoms (crossed atom at the center). N atoms are gray, Ti are blue and O atoms are marked red. Visualized by VESTA [37]. (For interpretation of the references to color in this figure legend, the reader is referred to the web version of this article.)

The relative intensity ratios of the five fitted components for all films are shown in the Fig. 4(a) and Table 1. The relative intensity ratio of the TiN component is the dominating one up to ~22 at.% O content and is decreasing with increasing O content over the whole composition range. The relative intensity ratio of the $TiON^1$ component increases up to ~30% at 18.5 at.% O and saturates at this level for higher oxygen concentrations. Similarly, the relative intensity ratio of the $TiON^2$ component is also increasing with the O content over the investigated composition range. However, contrary to the $TiON^1$ the increase of the $TiON^2$ component is moderate at low O contents and then increases monotonically

above 15 at.% O. The intensity ratio of the satellite peak is ~20%, similar for all here probed samples. The N_2 component is negligible in films with low O content and only becomes apparent in films with more than 15 at.% O, however its relative intensity is only around 5% even in the O-rich films. The intensities of the TiN, TiON[1] and TiON[2] components are renormalized to sum to 1 and shown in Fig. 4(b).

The obtained relative intensity versus O concentration trends are in a very good agreement with the theoretical expectations depicted in Fig. 4(c) for the relative intensities of the $N^{nV_{Ti}}$ components as a function of the amount of vacancies on the metal sublattice δ, where, assuming a random vacancy distribution, the probability of the N atom to have n Ti vacancies in the first coordination shell is

$$P^{N^{nV_{Ti}}}(\delta) = \binom{6}{n}\delta^n(1-\delta)^{6-n}. \quad (1)$$

The good agreement between the theoretical prediction and observed trends together with the very good agreement between the experimental and theoretical BE shifts is a direct evidence that the TiN, TiON[1] and TiON[2] components correspond to N atoms with 0, 1 and 2 close Ti vacancies respectively.

A discrepancy between prediction and experiment is visible at small O contents. If TiN, TiON[1] and TiON[2] components indeed directly correspond to $N^{0V_{Ti}}$, $N^{1V_{Ti}}$ and $N^{2V_{Ti}}$ components, their relative intensity ratios should be 1, 0 and 0 for pure TiN respectively, which is not the case. This disagreement is caused by the surface oxidation from atmospheric exposure. Greczynski and Hultman [35] report the surface oxynitride peak to be shifted by 1.05 eV to lower BEs from the main TiN peak, which causes an overestimation of the $N^{2V_{Ti}}$ and potentially of the $N^{1V_{Ti}}$ component. This is visible also in Fig. 2(a) and (b). At similar O contents the experimental TiON[1] and TiON[2] components are much stronger than the $N^{1V_{Ti}}$ and $N^{2V_{Ti}}$ calculated components, due to the additional surface oxidation in the experiment. In fact, it was previously reported that Ti vacancies are formed at the surface during oxidation of TiN [38] which is consistent with the findings presented herein.

There is no direct evidence for the presence of a $N^{3V_{Ti}}$ component in the experimental data which is likely caused by its relatively small population: assuming the random vacancy distribution, the $N^{3V_{Ti}}$ ratio is less than 10% at 20% metal vacancies on the metal sublattice. Furthermore, an energy penalty of 0.68 eV and 0.31 eV was reported for close Ti vacancies on (110) and (100) chains [39]. This energetic penalty further reduces the ratio of the $N^{3V_{Ti}}$ component at low Ti vacancy concentrations.

Before any quantification is possible, the influence of the surface oxidation from the atmospheric exposure has to be corrected for. Greczynski et al. [25] showed, that for pure TiN, four regions at the surface are present: the carbon contamination on top, pure oxide layer and a transition oxynitride layer which evolve due to atmosphere exposure and a bulk-like nitride (oxynitride in our case) region at the bottom. Since the N 1s peak is used to estimate the vacancy concentrations, it is possible to ignore the surface oxide layer as there is no nitrogen present, however the influence of the oxynitride transition layer needs to be taken into account, otherwise the amount of vacancies will be grossly overestimated.

The here applied correction procedure rests on the assumption that the oxidation of all samples is similar as the venting procedure and sample transport to the XPS were similar for all samples. Hence, it is reasonable to assume that the ratio of the nitrogen in the transitional oxynitride region to the nitrogen in the bulk-like region is constant for all of the samples. Therefore, we fit the component curves as shown in the Fig. 4(b) with functions similar to Eq. (1). However, a constant offset was applied to account for signal contributions due to surface oxidation by atmospheric exposure.

Since the experimental $N^{0V_{Ti}}$, $N^{1V_{Ti}}$ and $N^{2V_{Ti}}$ are normalized, the fitting functions are normalized as well

$$f^{N^{0V_{Ti}}}_{norm}(\delta) = \frac{P^{N^{0V_{Ti}}}(\delta)}{P^{N^{0V_{Ti}}}(\delta) + P^{N^{1V_{Ti}}}(\delta) + P^{N^{2V_{Ti}}}(\delta)} - C_1 - C_2, \quad (2)$$

$$f^{N^{1V_{Ti}}}_{norm}(\delta) = \frac{P^{N^{1V_{Ti}}}(\delta)}{P^{N^{0V_{Ti}}}(\delta) + P^{N^{1V_{Ti}}}(\delta) + P^{N^{2V_{Ti}}}(\delta)} + C_1, \quad (3)$$

$$f^{N^{2V_{Ti}}}_{norm}(\delta) = \frac{P^{N^{2V_{Ti}}}(\delta)}{P^{N^{0V_{Ti}}}(\delta) + P^{N^{1V_{Ti}}}(\delta) + P^{N^{2V_{Ti}}}(\delta)} + C_2, \quad (4)$$

where C_1 and C_2 take the effect of surface oxidation due to atmosphere exposure into account. It is furthermore assumed during the fitting of C_1 and C_2 the relationship between vacancy concentration and oxygen content can be described by a constant c, $\delta = c[O]$, a free parameter in the fit. The resulting fitted values of C_1 and C_2 are 5.3% and 8.3%.

With the component ratios corrected for the surface oxidation due to atmospheric exposure, the vacancy population can be estimated. Using the three TiN, TiON[1] and TiON[2] components, it is possible to obtain not only the vacancy concentration, but also their distribution, i.e., information about clustering or separation of the vacancies. However, for simplicity an averaging scheme for the values obtained from the separate components is used, while still assuming the random distribution. This approach searches for a δ, for which squared weighted differences between the theoretical $N^{0V_{Ti}}$, $N^{1V_{Ti}}$, $N^{2V_{Ti}}$ and experimental TiN, TiON[1], TiON[2] ratios is minimized, i.e., to find the minimum of a following function

$$\begin{aligned} g(\delta) = &\left(f^{N^{0V_{Ti}}}_{norm}(\delta) - f^{TiN}\right)^2\left(\frac{1}{\sigma^{TiN}}\right)^2 \\ &+\left(f^{N^{1V_{Ti}}}_{norm}(\delta) - f^{TiON^1}\right)^2\left(\frac{1}{\sigma^{TiON^1}}\right)^2 \\ &+\left(f^{N^{2V_{Ti}}}_{norm}(\delta) - f^{TiON^2}\right)^2\left(\frac{1}{\sigma^{TiON^2}}\right)^2, \end{aligned} \quad (5)$$

where f^{TiN}, f^{TiON^1}, f^{TiON^2} and σ^{TiN}, σ^{TiON^1}, σ^{TiON^2} are the fitted component ratios and their uncertainties for a specific O concentration.

The vacancy concentration estimates using the previously described method are summarized in Fig. 6. The results show a lin-

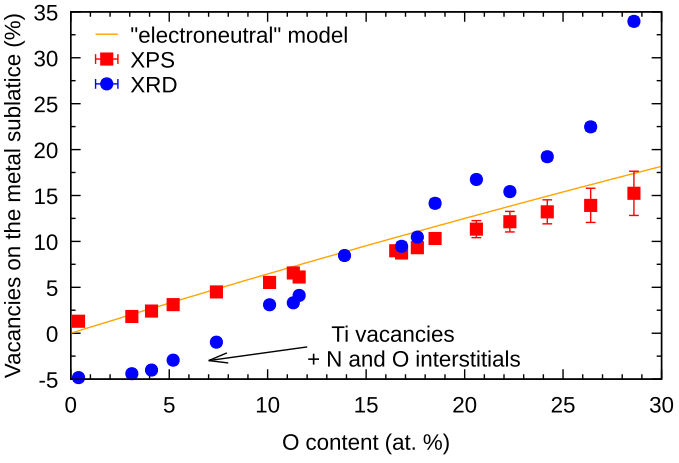

Fig. 6. Vacancy concentrations as estimated using the here developed XPS method. Simple estimate based on XRD lattice parameters is added for comparison, as well as a theoretical line for perfectly electroneutral composition (assuming +3, −3 and −2 oxidation number for Ti, N and O respectively). All of the models assume that the vacancies are the only defects present in the films. This is not perfectly satisfied below 13 at.% O. See SM Section S4 and S7 for more details.

ear increase over the whole oxygen composition range, from 1.3% of vacancies on the metal sublattice at 0.4 at.% of O to 15.2% of vacancies on the metal sublattice at 28.6%. of O and are in a perfect agreement with the simple electroneutral model. The simpler estimate of the composition dependent vacancy concentrations based on XRD lattice parameter replicate the trend but exhibits local deviations to both the electroneutral model as well as the composition dependent vacancy model based on the XPS data. While potential causes for the aforementioned local deviations are discussed in SM Section 7, the here presented results confirm that the Ti vacancies are inherently present in and stabilize the cubic titanium oxynitride and give further support to the previously proposed simple electroneutrality model [1,12]. Furthermore it is evident that the population of Ti vacancies in $Ti_{1-\delta}O_xN_{1-x}$ for up to 28.6 at.% O can be quantified with the here proposed model utilizing binding energy data obtained from the N 1s core spectra region via XPS.

4. Conclusions

Based on the *ab initio* and spectroscopy data, we have unequivocally established that the N 1s XPS signal of $Ti_{1-\delta}O_xN_{1-x}$ is sensitive to the presence of Ti vacancies and that the corresponding vacancy concentration can be quantified with the here proposed model. Spectroscopic analysis of the N 1s region of $Ti_{1-\delta}O_xN_{1-x}$ thin films with systematically varied oxygen concentration and therefore systematically varied Ti vacancy concentration revealed two components at approximately 0.6 eV and 1.1 eV lower binding energies with respect to the main TiN-like component. Using *ab initio* DFT calculations we established that these binding energy shifts are caused by the presence of 1 and 2 Ti vacancies in the first coordination shell of N atoms respectively. A theoretical model was proposed to quantify the vacancy concentration based on the relative ratios of the three N 1s components. As surface oxidation of the $Ti_{1-\delta}O_xN_{1-x}$ films also affect the N 1s binding energy, the corresponding signal contribution from the oxidized surface was taken into account. The so estimated XPS vacancy concentrations are consistent with the theoretical electroneutral model based on textbook oxidation states.

Declaration of Competing Interest

The authors declare that they have no known competing financial interests or personal relationships that could have appeared to influence the work reported in this paper.

CRediT authorship contribution statement

Pavel Ondračka: Conceptualization, Formal analysis, Investigation, Methodology, Writing – original draft, Writing – review & editing, Visualization. **Marcus Hans:** Formal analysis, Investigation, Writing – review & editing, Visualization. **Damian M. Holzapfel:** Formal analysis, Investigation, Writing – review & editing, Visualization. **Daniel Primetzhofer:** Formal analysis, Investigation, Writing – review & editing, Funding acquisition. **David Holec:** Conceptualization, Supervision, Writing – review & editing. **Jochen M. Schneider:** Conceptualization, Supervision, Project administration, Writing – review & editing, Funding acquisition.

Acknowledgments

This research was funded by German Research Foundation (DFG, SFB-TR 87/3) “Pulsed high power plasmas for the synthesis of nanostructured functional layer”. The authors acknowledge financial support from the Swedish research council, VR-RFI (contracts #821-2012-5144 & #2017-00646_9), and the Swedish Foundation for Strategic Research (SSF, contract RIF14-0053) for the operation of the tandem accelerator at Uppsala University. The authors also gratefully acknowledge the computing time granted by the JARA Vergabegremium and provided on the JARA Partition part of the supercomputer CLAIX at RWTH Aachen University (project JARA0151).

Supplementary material

Supplementary material associated with this article can be found, in the online version, at doi:10.1016/j.actamat.2022.117778.

References

[1] M. Hans, M. to Baben, D. Music, J. Ebenhöch, D. Primetzhofer, D. Kurapov, M. Arndt, H. Rudigier, J.M. Schneider, Effect of oxygen incorporation on the structure and elasticity of Ti-Al-O-N coatings synthesized by cathodic arc and high power pulsed magnetron sputtering, J. Appl. Phys. 116 (9) (2014) 2–7, doi:10.1063/1.4894776.
[2] H. Rueß, D. Music, A. Bahr, J.M. Schneider, Effect of chemical composition, defect structure, and stress state on the elastic properties of $(V_{1-x}Al_x)_{1-y}N_y$, J. Phys. 32 (2) (2020) 025901, doi:10.1088/1361-648X/ab46df.
[3] D.M. Holzapfel, D. Music, M. Hans, S. Wolff-Goodrich, D. Holec, D. Bogdanovski, M. Arndt, A.O. Eriksson, K. Yalamanchili, D. Primetzhofer, C.H. Liebscher, J.M. Schneider, Enhanced thermal stability of (Ti,Al)N coatings by oxygen incorporation, Acta Mater. 218 (2021) 117204, doi:10.1016/j.actamat.2021.117204.
[4] T. Lee, K. Ohmori, C.-S. Shin, D.G. Cahill, I. Petrov, J.E. Greene, Elastic constants of single-crystal $TiN_x(001)$ ($0.67 \leq x \leq 1.0$) determined as a function of x by picosecond ultrasonic measurements, Phys. Rev. B 71 (14) (2005) 144106, doi:10.1103/PhysRevB.71.144106.
[5] C.S. Shin, D. Gall, N. Hellgren, J. Patscheider, I. Petrov, J.E. Greene, Vacancy hardening in single-crystal $TiN_x(001)$ layers, J. Appl. Phys. 93 (10) (2003) 6025–6028, doi:10.1063/1.1568521.
[6] H. Kindlund, D. Sangiovanni, J. Lu, J. Jensen, V. Chirita, J. Birch, I. Petrov, J. Greene, L. Hultman, Vacancy-induced toughening in hard single-crystal $V_{0.5}Mo_{0.5}N_x$/MgO(001) thin films, Acta Mater. 77 (2014) 394–400, doi:10.1016/j.actamat.2014.06.025.
[7] M. to Baben, M. Hans, D. Primetzhofer, S. Evertz, H. Ruess, J.M. Schneider, Unprecedented thermal stability of inherently metastable titanium aluminum nitride by point defect engineering, Mater. Res. Lett. 5 (3) (2017) 158–169, doi:10.1080/21663831.2016.1233914.
[8] N. Koutná, D. Holec, O. Svoboda, F.F. Klimashin, P.H. Mayrhofer, Point defects stabilise cubic Mo-N and Ta-N, J. Phys. D 49 (37) (2016) 375303, doi:10.1088/0022-3727/49/37/375303.
[9] K. Balasubramanian, S. Khare, D. Gall, Vacancy-induced mechanical stabilization of cubic tungsten nitride, Phys. Rev. B 94 (17) (2016) 36–38, doi:10.1103/PhysRevB.94.174111.
[10] J. Gubicza, Characterization methods of lattice defects, in: Defect Structure and Properties of Nanomaterials, Elsevier, 2017, pp. 27–57, doi:10.1016/B978-0-08-101917-7.00002-5.
[11] P.S. Bagus, F. Illas, G. Pacchioni, F. Parmigiani, Mechanisms responsible for chemical shifts of core-level binding energies and their relationship to chemical bonding, J. Electron. Spectrosc. 100 (1–3) (1999) 215–236, doi:10.1016/S0368-2048(99)00048-1.
[12] K.P. Shaha, H. Rueß, S. Rotert, M. to Baben, D. Music, J.M. Schneider, Nonmetal sublattice population induced defect structure in transition metal aluminum oxynitrides, Appl. Phys. Lett. 103 (22) (2013) 1–6, doi:10.1063/1.4833835.
[13] N. Schalk, J.F.T.S. Fotso, D. Holec, A. Fian, G. Jakopic, V.L. Terziyska, R. Daniel, C. Mitterer, Microstructure, mechanical and optical properties of TiAlON coatings sputter-deposited with varying oxygen partial pressures, J. Phys. D 49 (2) (2016) 025307, doi:10.1088/0022-3727/49/2/025307.
[14] N. Schalk, J.F.T.S. Fotso, D. Holec, G. Jakopic, A. Fian, V. L. Terziyska, R. Daniel, C. Mitterer, Influence of varying nitrogen partial pressures on microstructure, mechanical and optical properties of sputtered TiAlON coatings, Acta Mater. 119 (2016) 26–34, doi:10.1016/j.actamat.2016.08.007.
[15] T. Duguet, C. Bessaguet, M. Aufray, J. Esvan, C. Charvillat, C. Vahlas, C. Lacaze-Dufaure, Toward a computational and experimental model of a poly-epoxy surface, Appl. Surf. Sci. 324 (2015) 605–611, doi:10.1016/j.apsusc.2014.10.096.
[16] T. Duguet, A. Gavrielides, J. Esvan, T. Mineva, C. Lacaze-Dufaure, DFT simulation of XPS reveals Cu/epoxy polymer interfacial bonding, J. Phys. Chem. C 123 (51) (2019) 30917–30925, doi:10.1021/acs.jpcc.9b07772.
[17] A. Gavrielides, T. Duguet, J. Esvan, C. Lacaze-Dufaure, P.S. Bagus, A poly-epoxy surface explored by Hartree–Fock δSCF simulations of C1s XPS spectra, J. Chem. Phys. 145 (7) (2016) 074703, doi:10.1063/1.4960762.
[18] A. Panepinto, D. Cornil, P. Guttmann, C. Bittencourt, J. Cornil, R. Snyders, Fine control of the chemistry of nitrogen doping in TiO_2: a joint experimental and theoretical study, J. Phys. Chem. C 124 (31) (2020) 17401–17412, doi:10.1021/acs.jpcc.0c05003.
[19] C.-C. Lee, J. Yoshinobu, K. Mukai, S. Yoshimoto, H. Ueda, R. Friedlein, A. Fleurence, Y. Yamada-Takamura, T. Ozaki, Single-particle excitation of core states in epitaxial silicene, Phys. Rev. B 95 (11) (2017) 115437, doi:10.1103/PhysRevB.95.115437.
[20] P. Ondračka, D. Nečas, M. Carette, S. Elisabeth, D. Holec, A. Granier, A. Goullet, L. Zajíčková, M. Richard-Plouet, Unravelling local environments in mixed TiO_2-

SiO_2 thin films by XPS and ab initio calculations, Appl. Surf. Sci. 510 (2020) 145056, doi:10.1016/j.apsusc.2019.145056.
[21] A. Aarva, V.L. Deringer, S. Sainio, T. Laurila, M.A. Caro, Understanding X-ray spectroscopy of carbonaceous materials by combining experiments, density functional theory, and machine learning. Part I: fingerprint spectra, Chem. Mater. 31 (22) (2019) 9243–9255, doi:10.1021/acs.chemmater.9b02049.
[22] C.C. Lee, B. Feng, M. D'Angelo, R. Yukawa, R.Y. Liu, T. Kondo, H. Kumigashira, I. Matsuda, T. Ozaki, Peculiar bonding associated with atomic doping and hidden honeycombs in borophene, Phys. Rev. B 97 (7) (2018) 1–5, doi:10.1103/PhysRevB.97.075430.
[23] K. Yamazaki, Y. Maehara, C.C. Lee, J. Yoshinobu, T. Ozaki, K. Gohara, Atomic structure and local electronic states of single Pt atoms dispersed on graphene, J. Phys. Chem. C 122 (48) (2018) 27292–27300, doi:10.1021/acs.jpcc.8b04529.
[24] M. to Baben, Oxygen Incorporation in MAX Phases and TiAlN and Elastic Properties of Nanolaminates, RWTH Aachen University, Aachen, 2013 Ph.D. thesis. https://publications.rwth-aachen.de/record/211570/files/4454.pdf
[25] G. Greczynski, S. Mráz, L. Hultman, J.M. Schneider, Venting temperature determines surface chemistry of magnetron sputtered TiN films, Appl. Phys. Lett. 108 (4) (2016), doi:10.1063/1.4940974.
[26] C. Azina, S. Mráz, G. Greczynski, M. Hans, D. Primetzhofer, J.M. Schneider, P. Eklund, Oxidation behaviour of V_2AlC MAX phase coatings, J. Eur. Ceram. Soc. 40 (13) (2020) 4436–4444, doi:10.1016/j.jeurceramsoc.2020.05.080.
[27] M.A. Sortica, V. Paneta, B. Bruckner, S. Lohmann, M. Hans, T. Nyberg, P. Bauer, D. Primetzhofer, Electronic energy-loss mechanisms for H, He, and Ne in TiN, Phys. Rev. A 96 (3) (2017) 032703, doi:10.1103/PhysRevA.96.032703.
[28] P. Hohenberg, W. Kohn, Inhomogeneous electron gas, Phys. Rev. 136 (3B) (1964) B864–B871, doi:10.1103/PhysRev.136.B864.
[29] W. Kohn, L.J. Sham, Self-consistent equations including exchange and correlation effects, Phys. Rev. 140 (4A) (1965) A1133–A1138, doi:10.1103/PhysRev.140.A1133.
[30] A. Zunger, S.H. Wei, L.G. Ferreira, J.E. Bernard, Special quasirandom structures, Phys. Rev. Lett. 65 (3) (1990) 353–356, doi:10.1103/PhysRevLett.65.353.
[31] G. Kresse, J. Furthmüller, Efficiency of ab-initio total energy calculations for metals and semiconductors using a plane-wave basis set, Comput. Mater. Sci 6 (1) (1996) 15–50, doi:10.1016/0927-0256(96)00008-0.
[32] G. Kresse, J. Furthmüller, Efficient iterative schemes for ab initio total-energy calculations using a plane-wave basis set, Phys. Rev. B 54 (16) (1996) 11169–11186, doi:10.1103/PhysRevB.54.11169.
[33] P. Blaha, K. Schwarz, F. Tran, R. Laskowski, G.K.H. Madsen, L.D. Marks, WIEN2k: an APW + lo program for calculating the properties of solids, J. Chem. Phys. 152 (7) (2020) 074101, doi:10.1063/1.5143061.
[34] P. Ondračka, NOMAD dataset: *ab initio*-guided X-ray photoelectron spectroscopy quantification of Ti vacancies in $Ti1-\delta O_xN_{1-x}$ thin films - ab initio data, 2021. doi:10.17172/NOMAD/2021.10.22-1.
[35] G. Greczynski, L. Hultman, Self-consistent modelling of X-ray photoelectron spectra from air-exposed polycrystalline TiN thin films, Appl. Surf. Sci. 387 (2016) 294–300, doi:10.1016/j.apsusc.2016.06.012.
[36] S. Tougaard, Quantitative analysis of the inelastic background in surface electron spectroscopy, Surf. Interface Anal. 11 (9) (1988) 453–472, doi:10.1002/sia.740110902.
[37] K. Momma, F. Izumi, VESTA 3 for three-dimensional visualization of crystal, volumetric and morphology data, J. Appl. Crystallogr. 44 (6) (2011) 1272–1276, doi:10.1107/S0021889811038970.
[38] J. Zimmermann, M.W. Finnis, L.C. Ciacchi, Vacancy segregation in the initial oxidation stages of the TiN(100) surface, J. Chem. Phys. 130 (13) (2009), doi:10.1063/1.3105992.
[39] L. Tsetseris, N. Kalfagiannis, S. Logothetidis, S.T. Pantelides, Structure and interaction of point defects in transition-metal nitrides, Phys. Rev. B 76 (22) (2007) 224107, doi:10.1103/PhysRevB.76.224107.